



Ionic surfactants of different dipole moments as anti-solvent additives for air-processing MAPbI_{3-x}Cl_x perovskite thin films

Jaquelina Camacho-Cáceres¹, Mario A. Millán-Franco¹, Melvia Carinne Mejía-Vázquez¹, Carlos Fabián Arias-Ramos¹, Asiel N. Corpus-Mendoza^{1,2}, Mario A. Rodríguez-Rivera³, María Elena Nicho⁴, Mérida Sotelo-Lerma⁵, and Hailin Hu^{1,*}

¹ Instituto de Energías Renovables (IER), Universidad Nacional Autónoma de México (UNAM), Priv.Xochicalco S/N, 62580 Temixco, Morelos, Mexico

² CONAHCYT-IER-UNAM, Temixco, Mexico

³ Centro de Investigación en Óptica, Lomas del Bosque 115, Lomas del Campestre, 37150 León, Guanajuato, Mexico

⁴ Centro de Investigación en Ingeniería y Ciencias Aplicadas, Universidad Autónoma del Estado de Morelos, Av. Universidad 1001, 62209 Cuernavaca, Morelos, Mexico

⁵ Departamento de Investigación en Polímeros y Materiales, Universidad de Sonora, Blvd. Luis Encinas y Rosales S/N, 83000 Hermosillo, Sonora, Mexico

Received: 22 August 2023

Accepted: 18 November 2023

Published online:
10 December 2023

© The Author(s), 2023

ABSTRACT

Three ionic surfactants, didodecyldimethylammonium bromide (DDABr), sodium lauryl ether sulfate (NaLES) and sodium lauryl sulfate (NaLS), with different dipole moment values: 0.907, 17 and 212 Debye, respectively, have been used as anti-solvent additives to remove the moisture from perovskite precursor solutions. The three additives impact in different ways on the crystallinity, wettability and morphology of perovskite thin films, as well as on the stability and efficiency of air-processed perovskite solar cells (PSCs). The hydrophobic groups of the additives at the surface of perovskite thin films help to increase the stability of PSCs, especially DDABr of the lowest dipole moment. On the other hand, NaLES, of the highest dipole moment, is the most efficient to extract moisture from the perovskite precursor coatings, increasing the average power conversion efficiency (PCE) of NaLES-based PSCs from $16.16 \pm 0.94\%$ to $17.21 \pm 0.32\%$ in comparison with that of the reference. Furthermore, the synergy between NaLES and the perovskite precursor additive, KI, achieves the best photovoltaic performance of the PSCs, leading to an average PCE of 17.42% and the best PCE of 18.75%. It is concluded that ionic surfactants of different dipole moments are good candidates as anti-solvent additives to improve the efficiency and stability of air-processed PSCs.

Address correspondence to E-mail: hzh@ier.unam.mx

1 Introduction

Since the first report of Miyasaka and collaborators in 2009 on the use of hybrid perovskite in dye sensitized solar cells [1], great achievements have been reported in solution prepared all solid perovskite solar cells (PSCs). In recent years the power conversion efficiency (PCE) record of PSCs, prepared under inert conditions has achieved up to 25.8% in small area [2]. In addition to their excellent optical and electrical properties [3], the success of hybrid perovskites as a photovoltaic material is mainly due to the continuously worldwide research works in understanding the formation process of highly crystalline and compact perovskite thin films through diverse defect reduction or passivation techniques [4]. However, when carrying out the manufacture of perovskites in high relative humidity ambient conditions, the main problem is the moisture in the environment that deteriorates the quality of perovskite thin films and the stability of the PSCs [5]. From scale-up and commercialization point of view, it is essential the development of air-processed and stable PSCs [5–9]. Techniques such as composition engineering, additive engineering, solvent engineering, interface engineering and other methods, have been employed to achieve the passivation effect and improve the performance and stability of ambient processed PSCs [7].

Additives are usually incorporated in perovskite precursor solutions during PSC fabrication. They could coordinate with different species of the solutions to control the nucleation and growth of perovskite compounds, and their presence in the solid perovskite films could protect them from the environmental moisture and inhibit the degradation process [7]. It is seen that 1,8-diiodooctane (DIO) additive could induce multi-stage intermediate crystallization phases and increases the activation energy for nucleation and growth, which postpones the perovskite phase transformation time and broadens the transition zone [10]. Additives such as elemental iodine, organic surfactants or surfactants, and Group 1 metal compounds have been reported to passivate recombination trap centers [11]. Surfactants are characterized by the capacity of modifying the surface tension between two phases, either liquid–liquid, liquid–solid or liquid–gas. Such a property is provided by the particular molecular compositions of the surfactants, which could consist in hydrophobic terminals (water-fear, alkyl chains, for example) or hydrophilic terminals (water-friend, ionic groups, for example), and can be classified as

non-ionic, anionic, cationic or amphoteric (carrying both positive and negative charges, also called zwitterionic) [12]. Specially, sodium dodecyl benzene sulfonate [13], 1- α -phosphatidylcholine [14], surfactant-like monoammonium zinc porphyrin [15], cetyl trimethyl ammonium bromide [16], poly(oxyethylene tridecyl ether) [17], non-ionic surfactant polyoxyethylene (20) sorbitan monolaurate [18], zwitterionic surfactant tetradecyldimethyl(3-sulfopropyl)ammonium hydroxide [19], heptadecafluorooctanesulfonic acid tetraethylammonium salt [20], among the others, have been reported to be multifunctional chemical additives to simultaneously improve the efficiency and stability in air of PSCs. In addition, potassium iodide (KI) has also been reported as hysteresis minimizer in perovskite solar cells [21–23].

On the other hand, solvent engineering can either refer to refining the solvents used in the perovskite precursor solutions, or the dynamic dripping of an anti-solvent during the spin-coating procedure [7]. More specifically, anti-solvent is usually dripped onto the perovskite precursor coating still in spin-coating process to remove the perovskite precursor solvents and create a supersaturated solution, resulting in an accelerated nucleation process of perovskite crystals and posterior formation of a compact and pinhole-free perovskite thin film with large grain sizes [7]. However, the control of perovskite crystallization is not easy through a single anti-solvent, and additives have been combined with anti-solvents to improve perovskite crystallization, reduce defect density and enhance the interfacial hydrophobic characteristic of the perovskite films [24]. Very small amounts of acetylacetone (AA) [24] and 4-*tert*-butylpyridine (TBP) [25] have been added in a green anti-solvent of ethyl acetate (EA) and improved efficiency and stability in air-processed methylammonium lead tri-iodide (MAPbI₃)-based PSCs.

Considering that the anti-solvents of lower polarity index, such as EA (4.4) accelerate the evaporation of the perovskite precursor solvents of higher polarity indexes, dimethylformamide (DMF, 6.4) and dimethyl sulfoxide (DMSO, 7.2) [26], it is desirable that the additives in the anti-solvents could play a synergistic role in crystal nucleation, grain formation and moisture elimination during MaPbI_{x-3}Cl_x-based perovskite formation under ambient conditions. In this work, three environmentally friendly ionic surfactants of different dipole moments have been chosen as additives of EA-based anti-solvent solutions: sodium lauryl ether

sulfate (NaLES), sodium lauryl sulfate (NaLS) and didodecyldimethylammonium bromide (DDABr). All of them have both hydrophilic and hydrophobic terminal groups; the hydrophilic groups could help to catch and remove the moisture from the wet perovskite coating, and the hydrophobic groups ($\text{CH}_3(\text{CH}_2)_{10}-$) to improve the moisture resistance of the perovskite thin film. The results show that NaLES, with the largest dipole moment among the three, is more effective in reducing perovskite crystal dislocation density and increasing grain size, achieving an average PCE of 17.21% of the corresponding PSCs. Moreover, the combination of NaLES anti-solvent additive and KI, the perovskite precursor solution additive, leads to a synergistic effect in perovskite crystal growth under ambient conditions, resulting in an average PCE of 17.42% and the best PCE of 18.75%. The stability of the PSCs prepared with any of the three anti-solvent additives is improved after 30 min continuous illumination; the additive of the lowest dipole moment, DDABr, gives the highest hydrophobic perovskite surface and the lowest PCE loss of un-capsulated PSCs (5%) after a continuous light exposure under ambient conditions with 50% relative humidity (RH).

2 Experimental

2.1 Perovskite solar cell preparation

Glass slides coated with conductive fluorine-doped tin oxide (FTO, TEC-15, 15 Ω /square, Greatcell Solar) were cut and patterned with zinc and 3 M HCl. They were washed first with soap and water, rinsed with distilled water, followed by ultrasonic cleaning in acetone and in isopropyl alcohol for 15 min each. After drying in air, they were cleaned in UV/ozone equipment (Bioforce) for 20 min to eliminate possible organic traces at the surface of FTO.

An anhydrous titanium isopropoxide (Aldrich, 97%) solution in isopropyl alcohol was prepared and spin coated on top of the patterned FTO substrates at 3000 rpm for 30 s. Subsequently, the samples were heated at 100 °C for 5 min on a hot plate and then in a muffle at 450 °C for 30 min. After natural cooling, compact titanium dioxide thin films (c-TiO₂) of thickness of about 35 nm were formed on FTO.

A commercial TiO₂ nanoparticle paste (30NRD Titania Paste, Greatcell Solar) was diluted in anhydrous ethanol in a 1:6 weight ratio. The obtained solution

was spin-coated on top of c-TiO₂ at 4000 rpm for 30 s, followed by a thermal annealing in a muffle at 500 °C for 30 min and cooling down to room temperature. Mesoporous titanium dioxide films (mp-TiO₂) of thickness of about 300 nm were formed on top of c-TiO₂ by spin-coating at 4000 rpm for 30 s, followed by a thermal treatment in air 500 °C for 30 min.

The perovskite precursor solution for one-step method was prepared as follows: 3.4 mg of methyl ammonium chloride (MACl, Lumtec, $\geq 98\%$), 159 mg of methyl ammonium iodide (MAI, Lumtec, 99.5%), 461 mg of PbI₂ (Lumtec, 99.999%), 78.1 mg of dimethyl sulfoxide (DMSO, Aldrich 99.9%) and 600 mg of dimethylformamide (DMF, Aldrich 99.8%) were added in a vial, and stirred at 500 rpm in a magnetic stirrer for 20 h. For comparison purpose, some of the perovskite precursor solutions contained 5 μL of a 16.6 mg/mL potassium iodide (KI) solution in DMF, which equivaless to a concentration of 5 μmol .

The perovskite precursor solution was spin-coated on top of mp-TiO₂ at 5000 rpm. At 6 s of spinning time, 140 μL of anti-solvent of ethyl acetate (EA), with or without additive, was gently dripped on top of the coating in spinning. The spin process lasted for 20 s in total. The as-deposited coating samples were transferred to a hot plate at 100 °C and became dark perovskite solid films after 2 min of annealing. The scheme of one-step preparation of perovskite films is shown in Fig. 1a. All perovskite thin film deposition was carried out in an extraction hood, exposed to ambient conditions with a room temperature (T_a) of 24.0–27.5 °C and relative humidity (RH) of 44–53.3%. T_a and RH were recorded using a hygrometer UNI-T model UT333BT with error range of ± 1 °C for temperature and of $\pm 5\%$ for RH.

EA-based anti-solvent solutions with additives were prepared by mixing EA and surfactant stock solutions. Table 1 shows the molecular formula and dipole moment of the three surfactants as additives for EA-based anti-solvents: DDABr (powder, Aldrich, 99%), NaLS (powder, Cedrosa, 97.9%), and NaLES (liquid, Farmacia Paris, 26–29% in water–alcohol solution). The dipole moment values of the three molecules in a dissociated state were estimated using the software Avogadro. The surfactant stock solutions had a concentration of about 1 mg/mL, prepared by dissolving 5 mg of each surfactant in 5 mL of EA. 10 μL of deionized water was added in DDABr and NaLS solutions to help the dissolution of the powers in EA. All these surfactant stock solutions were sonicated for 10 min

Fig. 1 **a** One-step spin coating of perovskite thin films and **b** cross-sectional configuration of n-i-p perovskite solar cells prepared in this work

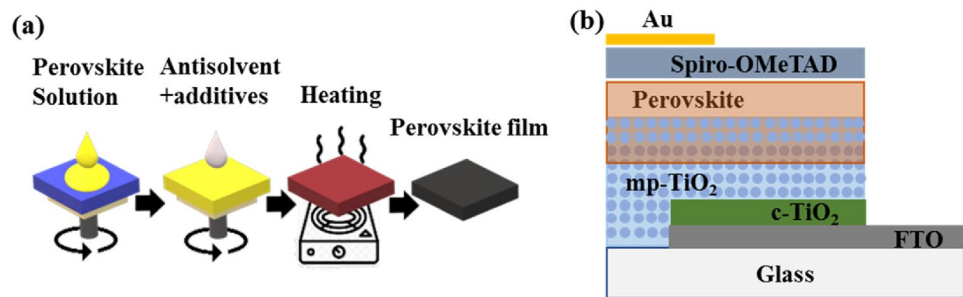


Table 1 Molecular formula and dipole moment of ethyl acetate (EA) and three different surfactants as additives in EA-based anti-solvent solution preparation

Additive in EA	Molecular formula	Dipole moment in dissociated state (Debye, <i>D</i>)
EA	CH ₃ CO ₂ CH ₂ CH ₃	0.331
Didodecyl dimethyl ammonium bromide (DDABr)	(CH ₃ (CH ₂) ₁₀ CH ₂) ₂ N(CH ₃) ₂ Br	0.907
Sodium lauryl ether sulfate (NaLES)	CH ₃ (CH ₂) ₁₀ CH ₂ (CH ₂ -O-CH ₂) _{<i>n</i>} -O-SO ₃ Na	212
Sodium lauryl sulfate (NaLS)	CH ₃ (CH ₂) ₁₀ CH ₂ O-SO ₃ Na	17

in an ultrasonic bath and the final surfactant stock solutions had a total volume of 5 mL approximately. The additive concentrations in each EA anti-solvent solutions were chosen as: 0.14, 0.21, 0.28 and 0.36 mg/mL. In total, 16 types of perovskite thin films (and solar cells) were prepared with different anti-solvent solutions.

To complete perovskite solar cell preparation, a 2,2',7,7'-tetrakis[*N,N*-di(4-methoxyphenyl)amino]-9,9'-spirobifluorene (spiro-MeOTAD) solution was prepared by adding 60 mg spiro-MeOTAD (Lumtec, 99.5%) in 750 μ L of chlorobenzene (Aldrich, 99%), plus 21.8 μ L of 4-*tert*-butylpyridine (Aldrich, 98%) and 13.4 μ L of 1.81 M bis(trifluoromethylsulfonyl)amine lithium salt (Li-TFSI) (Aldrich, 99%) in acetonitrile solution. The spiro-MeOTAD solution was stirred for 2 h at 500 rpm and deposited by spin coating on a perovskite thin film at 2500 rpm for 30 s in a glove box with 10% of RH. Finally, the gold contact was deposited by thermal evaporation in a high vacuum chamber ($\sim 5 \times 10^{-5}$ Torr). The perovskite solar cells (PSCs) prepared in this work had an n-i-p configuration, as shown in Fig. 1b.

2.2 Materials and device characterization

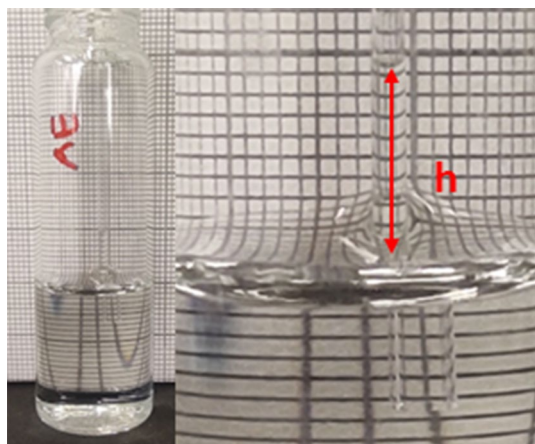
Surface tension (σ) of EA-based anti-solvent solutions, without and with the three surfactants of different

concentrations, was measured with the capillary lift method. Such method consists in putting a capillary tube of a known internal diameter into an anti-solvent solution of a known density (ρ). The tube maintained vertically inside the solution, without touching neither the bottom nor the wall of the solution container. For each type of anti-solvent solutions, pictures were taken to the capillary tube to measure the height of the liquid column inside the tube (h) compared to the liquid surface outside the tube (see the red arrow in Scheme 1 that represents such height). A millimeter sheet was used as background for the photography, and ImageJ software was used to determine the values of the height in each picture.

By considering that the amount of additives in the anti-solvent solutions is very small, we assume that the density of the EA-based anti-solvent solutions (ρ) remains as constant regardless of the additive's concentration. Then the dependence of the surface tension of the testing anti-solvent (σ) on ρ and h can be described with the following equation [27]:

$$2\sigma/R = \rho g h, \quad (1)$$

where the unit of σ is mN/m, R is the internal radius of the capillary tube (cm), the unit of ρ is g/cm³, g is the gravitational acceleration constant (cm/s²), and h is the height of the capillary column (cm).



Scheme 1 Capillary lift method to measure the surface tension of anti-solvent solutions (Color figure online)

Surface contact angle of a drop of water on the surface of a perovskite thin film was measured by taking high-resolution slow motion videos at 120 FPS with a Samsung A71 cell phone equipped with a 9280×694 pixel camera. With the help of the ImageJ software the contact angle was determined from the pictures. Thickness of thin solid films was measured by a contact profilometry (Ambios XP200).

Surface morphology of perovskite thin films was measured by a Scanning Electron Microscope (SEM, FESEM Hitachi S-5500). Surface roughness of perovskite thin films was analyzed with an Atomic Force Microscopy (AFM) in Bruker-Veeco Dimension Icon equipment. The measurement was carried out in ScanAsyst mode with a scanning speed of 0.977 Hz. The tip had a ScanAsyst HPI reference in rectangular shape with a radius of 4 ± 2 nm. Fourier Transform Infrared (FT-IR) spectroscopy (Nicolet iS50) in ATR mode was used to measure the vibrational spectra of perovskite thin films.

X-ray diffraction (XRD) patterns of perovskite thin films were obtained on a Rigaku diffractometer model DMAX2200 operated with a $\text{CuK}\alpha$ radiation source ($\lambda = 1.54056 \text{ \AA}$). The incident beam was at a grazing angle of 1.5° and the angle of the detector of the diffracted beams (2θ) varied from 10 to 70° . Average residual stresses were obtained from the crystallographic data using W.H. Hall method [28]. The dislocation densities were deduced from the average residual stress data using Williamson–Smallman method [29]. These methods were widely used in metallurgy for the analysis of bulk

material [30–32] and recently for thin film samples too [33, 34].

Current vs. voltage curves (I – V) of un-encapsulated perovskite solar cells were measured in an Oriel brand Sol3A class AAA solar simulator, in lighting conditions of AM1.5G, connected to a Keithley 2400 m. The light intensity was calibrated using a calibrated silicon reference cell (Newport). The voltage scanning speed was 0.15 V/s. Values of open circuit voltage (V_{OC}), short circuit current density (J_{SC}), fill factor (FF) and power conversion efficiency (PCE) were determined from I – V curves of each cell sample considering the effective area of the cells (0.104 cm^2). External quantum efficiency (EQE) measurements were performed on an Oriel QEPVSI-B system, calibrated with a Newport 71,889 photodetector. The stability measurements under continuous lighting were carried out in an Oriel solar simulator model XTRALIEN X200. All solar cell measurements were carried out under ambient conditions.

3 Results and discussion

The addition of surfactants as additives in ethyl acetate (EA) changes the surface tension of the resulting anti-solvent solutions. Figure 2a shows that the surface tension of EA is of 20.9 mN/m . After addition of DDABr, NaLES or NaLS in EA, the surface tension of all EA-additive solutions decreases with the concentration of the additives. For an additive concentration of 0.36 mg/mL , the surface tension is the smallest in the case of NaLES (18.6 mN/m), largest for NaLS (20.3 mN/m), and in-between for DDABr (19.2 mN/m). We assume that the three ionic surfactants have the hydrophilic terminals at the surface of the hydrophobic EA solutions, as illustrated in the inset of Fig. 2a, reducing the surface tension of the liquid at liquid/air interface.

To see the effect of the anti-solvents on the surface hydrophobicity of perovskite thin films, MAPbI_3 precursor solutions ($\text{MAI}:\text{PbI}_2 = 1:1$ molar ratio) with the same anti-solvents of Fig. 2a, were deposited on glass substrates by spin-coating and annealed at 100°C for 2 min. Contact angles of water drops on the surface of perovskite thin films were measured from the photographs of the drop/film interfaces (Fig. S1), and their values are shown in Fig. 2b. Compared to the perovskite films prepared with EA only anti-solvent, the presence of additives in EA significantly affect the contact angle values of water

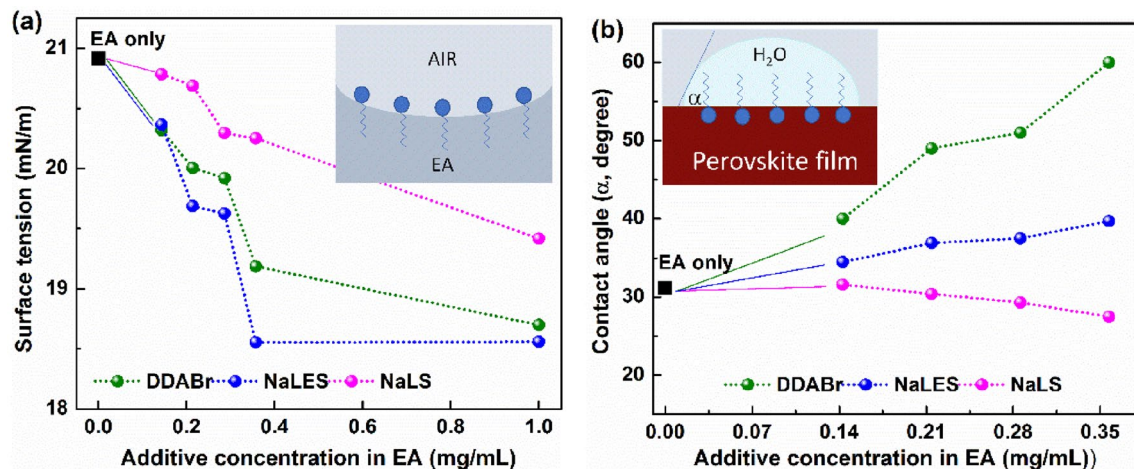


Fig. 2 **a** Surface tension values of ethyl acetate (EA)-based solutions, without or with three types of surfactant additives: DDABr, NaLES and NaLS, as functions of the additive concentration, varied from 0 (EA) to 1 mg/mL. **b** Contact angle values of water

drops at the surface of perovskite thin films as function of the additive type and concentration. The measurements were made under a relative humidity of about 70%

drops at the perovskite surface: DDABr and NaLES increase the contact angle, the first quickly and the second slowly, whereas NaLS keeps the same value for 0.14 mg/mL, and after that the contact angle reduces slightly. These results suggest that the three additives should be at the surface of perovskite thin films to increase their hydrophobicity; the excess of NaLS (>0.14 mg/mL) would do the opposite. It is important to note that the absolute values of contact angles reduce with the ambient RH; the data in Fig. 1b were obtained under a RH of about 70%, which were lower than those obtained under a RH of 50–60% [25].

Additionally, the presence or “fingerprint” of organic anti-solvent additives at the surface of the solid perovskite thin films could be identified with FTIR spectroscopy if the concentration of the additives in the anti-solvent solutions is sufficiently high, as reported elsewhere [25]. In this work, we choose NaLES to confirm the presence of the additive at the surface of the perovskite thin films. Figure S2 shows FT-IR spectra of the NaLES compound (green curve) and two perovskite thin films: one prepared with EA-only anti-solvent (blue curves) and another with EA-NaLES anti-solvent with a very high NaLES concentration in EA (1.4 mg/mL, red curves). The broad vibrational band observed at $1230\text{--}1120\text{ cm}^{-1}$ suggests the presence of NaLES at the surface of the perovskite sample prepared with such additive.

The influence of anti-solvent additives on the perovskite crystal nucleation and growth, as well as grain size distribution in perovskite thin films, is confirmed by XRD and SEM, respectively. Figure 3a shows the XRD patterns of the perovskite thin films prepared with four different anti-solvent solutions: EA only, EA+ DDABr, NaLES, or NaLS; the concentration of the additives in EA solvent is 0.14 mg/mL in all the cases. It is observed that all the film samples contain the perovskite crystal phase with the strongest intensities at (110), (220) and (310) crystalline planes. Figure 3b shows the average crystal size at 14.08° or (110) plane (D , red open squares) and the dislocation density (ρ , red open pentagons) of the perovskite thin films. Compared to EA only sample, the addition of the three anti-solvent additives impacts in different ways to the values of D and ρ . D increases from 59.1 nm (EA) to 70.5 nm (DDABr) or 67.1 nm (NaLES), or reduces from 59.1 nm (EA) to 53.3 nm (NaLS). Meanwhile, ρ value reduces from 3.8×10^5 (EA) to 2.4×10^5 Line/m² (DDABr), and increases from 3.8×10^5 (EA) to 7.3×10^5 (NaLES) or to 7.2×10^5 Line/m² (NaLS).

On the other hand, potassium iodide (KI) has been used as additive in perovskite precursor solutions to reduce the defect density and consequently, the hysteresis of PSCs [21–23]. In this work, we try to looking for the possible synergy between the perovskite precursor solution additive (KI) and the anti-solvent additives (DDABr, NaLES and NaLS). Figure 3c shows

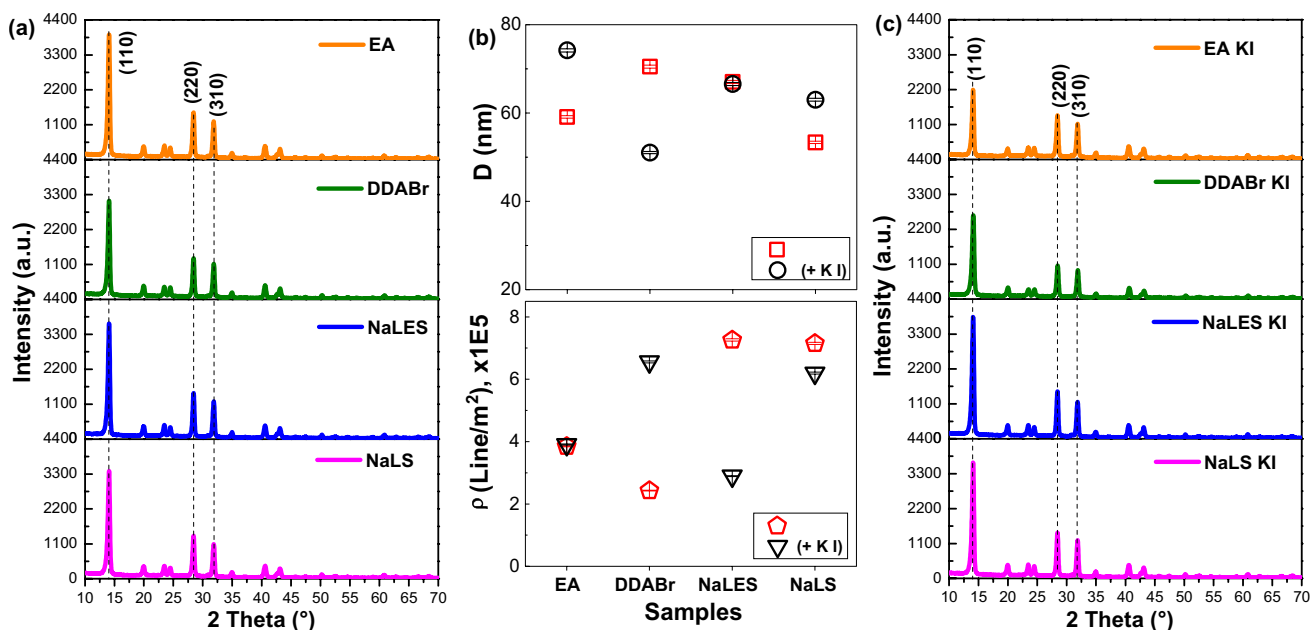


Fig. 3 **a** XRD patterns of the perovskite thin films prepared with four different anti-solvent solutions: EA only, EA+DDABr, NaLES or NaLS. The concentration of the additives in EA solvent is 0.14 mg/mL in all cases. **b** Perovskite crystal size (D) and dislocation density (ρ) at (110) plane of perovskite thin films. **c**

XRD patterns of the perovskite thin films prepared with the same four anti-solvent solutions, with 5 μmol of KI in the perovskite precursor solutions: EA-KI only, EA+DDABr-KI, NaLES-KI or NaLS-KI (Color figure online)

the XRD patterns of the perovskite thin films, prepared with the same four anti-solvent solutions as those in Fig. 3a, but with the addition of 5 μmol of KI in the perovskite precursor solutions. The corresponding samples are called as: EA-KI only, EA+DDABr-KI, NaLES-KI or NaLS-KI. Although the same crystalline structure is observed in all KI-based samples, the crystal sizes (D) of perovskite films are changed with the KI addition in the precursor solutions. From Fig. 3b, we can see that the addition of KI increases D values (black open circles) in two of four perovskite samples: EA-KI (from 59.1 to 74.2 nm) and NaLS-KI (from 53.3 to 63.0 nm), remains the D value of NaLES-KI, and reduces the D value of DDABr-KI samples (from 70.5 to 51.0 nm). On the other hand, the corresponding dislocation density (ρ) values of KI samples (black open down triangles in Fig. 3b) behave differently. ρ value remains the same in EA, increases significantly in DDABr-KI sample (from 2.4×10^5 to 6.6×10^5 Line/m²), and reduces in both NaLES and NaLS samples, showing the most significant reduction in NaLES sample (from 7.3×10^5 to 2.9×10^5 Line/m²). It seems that the effect of the combination of the precursor additive KI with the anti-solvent additives depends largely on the type of the anti-solvent additives. The

best combination is NaLES+KI, giving almost the same D and much smaller ρ value. The second best one is NaLS+KI, in which both D and ρ values are increased. The worst combination is DDABr+KI, showing decreased D and increased ρ values.

The ensemble of perovskite crystals forms perovskite grains, and the size and compactness of those grains can be observed in SEM surface morphology of perovskite thin films. Figure 4 shows SEM micrographs of perovskite thin films, with the grain size distribution (Φ) in $1 \mu\text{m}^2$ as the inset in each of them, prepared with EA-only (Fig. 4a), EA+DDABr (Fig. 5b), EA+NaLES (Fig. 4c) and EA+NaLS (Fig. 4d) anti-solvent solutions. The additive concentration in EA anti-solvent solutions is of 0.14 mg/mL in all the cases. Compared to the reference (EA), DDABr reduces the average gran sizes from 180 to 80 nm, NaLES gives similar grain size distribution and compactness, and NaLS keeps the same grain size distribution but leads to a less compact arrangement of perovskite grains.

Moreover, the effect of the perovskite precursor solution additive (KI) is clearly observed in the surface morphology of perovskite thin films. The SEM images in Fig. 5 indicate that the addition of KI in EA-only sample largely increases the perovskite grain size,

Fig. 4 SEM micrographs and grain size distributions in $1 \mu\text{m}^2$ of perovskite thin films prepared with: **a** EA, EA+, **b** DDABr, **c** NaLES, **d** NaLS. The concentration of the additives in EA was 0.14 mg/mL in all the cases

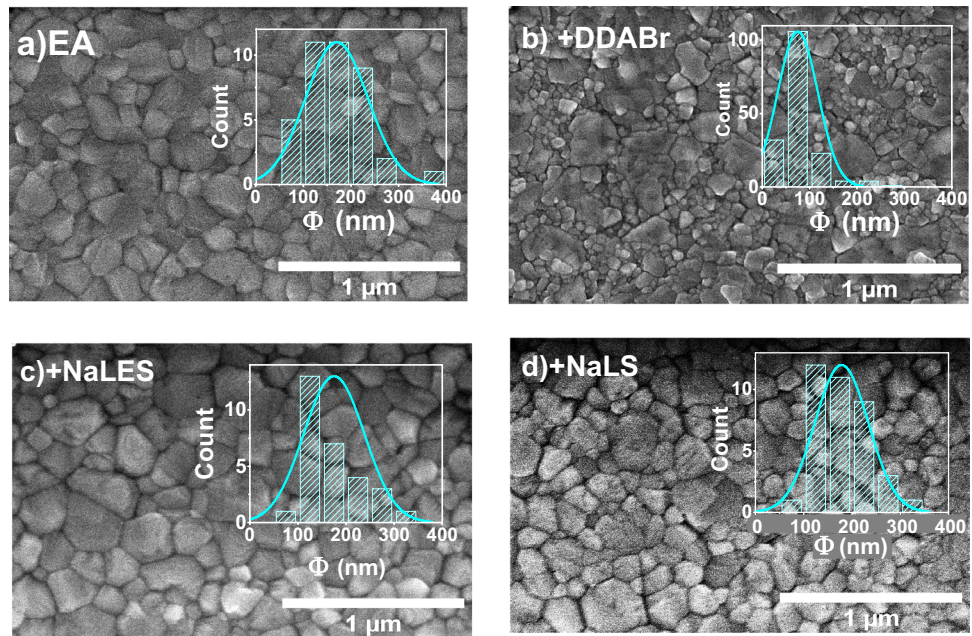
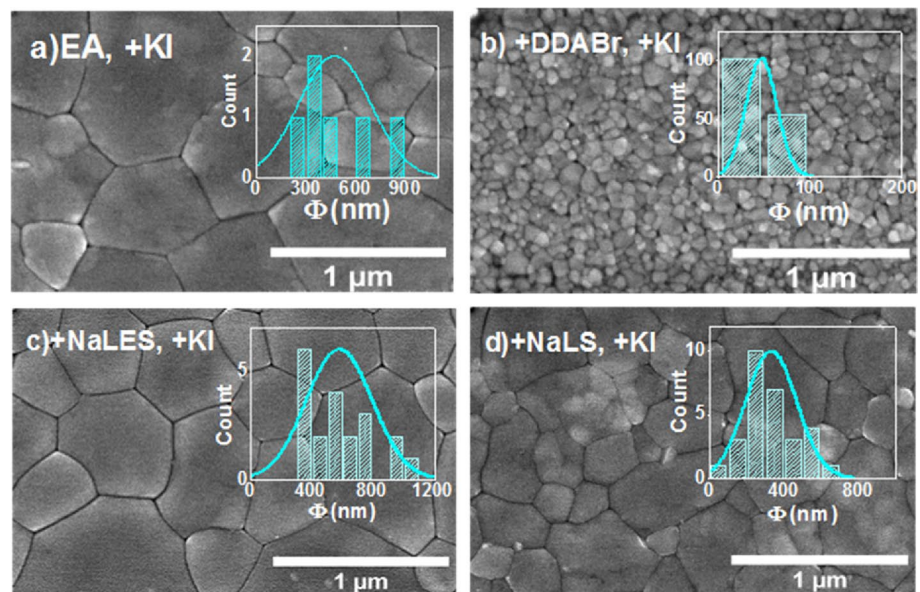


Fig. 5 SEM micrographs and grain size distributions in $1 \mu\text{m}^2$ of the perovskite thin films prepared with the same anti-solvent+additives as indicated in Fig. 4, with the difference in the addition of KI in the perovskite precursor solutions: **a** EA, **b** DDABr, **c** NaLES and **d** NaLS. The concentration of the additives in EA was 0.14 mg/mL in all the cases



from the range of 100–300 nm (Fig. 4a) to 400–1000 nm (Fig. 5a). On the contrary, the combination of the precursor solution additive KI with the DDABr anti-solvent additive notably reduces the grain size, from 25 to 200 nm (Fig. 4b) to 25–100 nm (Fig. 5b). The most successful case is the combination of KI with NaLES, resulting in the largest grain sizes (400–1200 nm) and the most compact surface of perovskite thin films (Fig. 5c), in comparison with that without KI (Fig. 4c). Finally, the combination of KI with NaLS leads to

intermediate results; the perovskite grain size distribution increases from 50–350 nm (Fig. 4d) to 50–750 nm (Fig. 5d).

From XRD and SEM results, it seems that the synergy between the precursor solution additive KI and the anti-solvent additives depends on the polarity of the anti-solvent additives. Without any anti-solvent additive, the addition of KI in the precursor solutions increases crystal as well as grain sizes in perovskite thin films, as reported elsewhere under different

perovskite thin film preparation conditions [21–23]. The same tendency is also observed in our perovskite thin films prepared with more polar anti-solvent additives, NaLES (dipole moment of 212 D) and NaLS (dipole moment of 17 D). However, the addition of the most hydrophobic anti-solvent additive DDABr (dipole moment of 0.903 D) reduces the perovskite grain sizes, without (Fig. 4b) or with the precursor solution additive KI (Fig. 5b). The function of an anti-solvent is to extract out the main solvents (DMF and DMSO) from the wet perovskite precursor coating to induce a supersaturated solution coating and enhance the perovskite crystal nucleation and growth process. From Angle contact results (Fig. 2b) it is evident that a large amount of DDABr molecules should be at the surface of perovskite thin films prepared with such additive. This fact suggests the possibility that a higher portion of DDABr molecules could have been remained inside the supersaturated perovskite precursor solutions, impeding the formation of larger grains in DDABr and DDABr–KI-based perovskite thin films.

Furthermore, the effect of the amount of anti-solvent additives on the crystallinity and morphology of perovskite thin films are shown in Figs. S3 and S4, respectively. As the additive concentration is increased from 0.14 to 0.36 mg/mL, both NaLES and NaLS increase D (red solid squares in Fig. S3b) and reduce ρ (red solid stars in Fig. S3b). However, DDABr reduces D and increases ρ as its concentration increases from 0.14 to 0.36 mg/mL in EA anti-solvent solution (Fig. S3b). The most important impact of the additive concentration is on the morphology of DDABr-based perovskite thin films, giving a porous surface (Fig. S4a), while NaLES and NaLS remain similar grain sizes and lead more compact surface (Fig. S4b and c, respectively). Additionally, the possible impact of the concentration of the anti-solvent additive on the surface roughness of perovskite thin films is verified with AFM images of perovskite film samples prepared using 0, 0.14 and 1.4 mg/mL of NaLES in EA anti-solvent solutions (Fig. S5). We observe that the addition of a small amount of NaLES (0.14 mg/mL) reduces 13.6% of the surface roughness (root mean square) of perovskite thin film in areas of $5 \mu\text{m}^2$, from 17.4 nm (without additive, Fig. S5a) to 15.2 nm (0.14 mg/mL of NaLES, Fig. S5b). However, a tenfold amount of NaLES (Fig. S5c) only reduces 16.6% of the surface roughness.

The influence of anti-solvent additives on photovoltaic performance of perovskite solar cells (PSCs) is shown in Fig. 6. The concentration of the additives

in EA is 0.14 mg/mL in all the perovskite thin films. The red boxes correspond to those PSCs prepared with EA, EA+ DDABr, EA+ NaLES or EA+ NaLS anti-solvents. Table 2 lists the average values \pm standard deviation of V_{OC} , J_{SC} , FF and PCE of all the PSCs in Fig. 6. Figure 7a shows the corresponding average current density (J) versus voltage (V) curves of these four types of PSCs under illumination. It is evident that all three anti-solvent additives improve the average FF values of the PSCs, compared to EA-only samples. Although DDABr-based samples excel in the average V_{OC} (1.01 V), they have a smaller average J_{SC} . And NaLS samples fail in all three photovoltaic parameters. The best photovoltaic performance is found in NaLES-based PSCs; they have the highest average FF values and the second best average V_{OC} and J_{SC} numbers, leading not only to the best average PCE but also the lowest standard deviation, $17.21 \pm 0.32\%$, in comparison with the EA-only samples ($16.15 \pm 0.94\%$). Table 2 also includes the results of the previous work [25], in which 4-tertbutyl-pyridine (tBP) was used as EA anti-solvent additive. It is observed that NaLES-based PSCs give higher average PCE than the tBP ones.

Furthermore, the effect of the concentration of the additives on the photovoltaic performance of the PSCs is also studied. With a higher additive concentration in EA anti-solvent solutions, 0.36 mg/mL, all the photovoltaic parameters have been reduced (Fig. S6, Table S1), with the largest lost in DDABr-based PSCs. In the case of DDABr additive, this loss is consistent with the crystallinity (Fig. S3) and morphology (Fig. S4) results of the corresponding perovskite thin films. In the cases of NaLES and NaLS, the reduced J_{SC} , FF and PCE values in those PSCs should come from a higher electrical resistance in perovskite thin films or at the perovskite/spiro-MeOTAD interface because of a larger amount of the additive molecules in the perovskite precursor coatings.

Figure 6 and Table 2 also include photovoltaic performance statistics of those PSCs (green boxes) prepared with the precursor solution additive KI and the four anti-solvent solutions, denoted as: EA+KI, +DDABr-KI, +NaLES-KI and +NaLS-KI samples. Figure 7b shows the average J – V curves of these PSCs under illumination. Comparing the green boxes with the red ones in Fig. 6, we can see that the addition of KI improves the EA-only samples' average FF, leading to a slightly higher average PCE. However, the combination of KI with DDABr is a total fiasco, followed by the NaLS-KI samples. The best photovoltaic

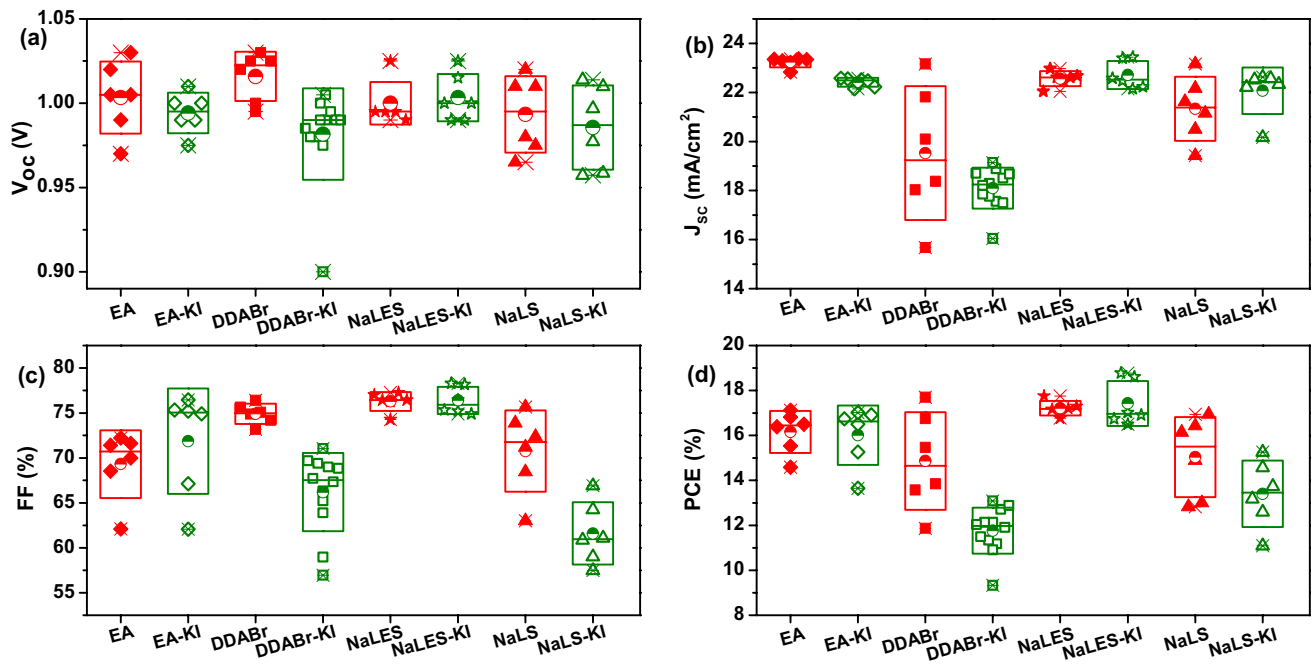


Fig. 6 Photovoltaic parameters: **a** V_{OC} , **b** J_{SC} , **c** FF and **d** PCE of perovskite solar cells prepared with different EA anti-solvent solutions (red boxes): EA, (EA+DDABr, (EA+)NaLES, (EA+)NaLS, as well as with the addition of KI in the perovskite pre-

cursor solutions (green boxes): EA-KI, +DDABr-KI, +NaLES-KI and +NaLS-KI. The concentration of the anti-solvent additives was 0.14 mg/mL (Color figure online)

performance of all PSCs in this work is found in the combination of NaLES and KI, just like the SEM image suggested (Fig. 5c); they have the second best average values in all three photovoltaic parameters (V_{OC} , J_{SC} and FF), and consequently the best average PCE of all the PSCs: $17.42 \pm 1.00\%$. The highest power conversion efficiency, $PCE_{MAX} = 18.75\%$, also comes from this group of PSCs, all prepared under ambient conditions. PSC samples prepared with NaLES anti-solvent additive show the best average $J-V$ curves, without (red stars in Fig. 7a) or with the precursor additive KI (green stars in Fig. 7b).

The photovoltaic performance of a solar cell is related to its electrical resistances in the equivalent circuit of the diode (solar cell), which can be obtained from the current–voltage ($I-V$) curve in dark of the cell sample. Highly efficient solar cells have small series resistance (R_S) and large shunt resistance (R_P). Table 2 lists R_S and R_P values of our PSCs, obtained from the respective dark $I-V$ curves. It is observed that NaLES is the only anti-solvent additive that achieves, at the same time, the reduction of R_S (from 68 to 40 Ω) and increase of R_P (from 2.74×10^5 to $3.33 \times 10^5 \Omega$), compared to EA only samples; DDABr reduces both R_S (59

Ω) and R_P ($1.83 \times 10^5 \Omega$) values, while NaLS increases both R_S (86 Ω) and R_P ($4.33 \times 10^5 \Omega$). The addition of the precursor solution additive KI increases R_P values of all our PSCs, regardless of the anti-solvent solution composition. And it reduces R_S values of three of the four types of PSCs: from 68 to 41 Ω (EA), from 40 to 16 Ω (NaLES) and from 86 to 33 Ω (NaLS), with the exception in the case of DDABr-KI: R_S increases from 59 to 135 Ω .

To envisage the correlation between microscopic and macroscopic properties of different types of PSCs, Fig. 8 compares the crystal (D) and grain size (G) of perovskite thin films with R_S and PCE of the corresponding PSCs; the blue symbols correspond to PSCs without KI, and red ones to the combination of the precursor additive KI and the anti-solvent additives. In EA and NaLES-based PSCs, larger D and G of perovskite thin films lead to lower R_S and higher PCE of the PSCs. On the other hand, smaller grain size G values in DDABr-based perovskite thin films are related to larger R_S and smaller PCE of the corresponding PSCs. The addition of KI notable increases G and reduces R_S in EA only, EA-NaLS and EA-NaLES samples, leading to the improved average PCE values

Table 2 Photovoltaic parameters (V_{OC} , J_{SC} , FF and PCE) of perovskite solar cells (PSCs) under illumination

EA +additive*, +KI	Average $V_{OC} \pm \delta$ (V)	Average $J_{SC} \pm \delta$ (mA/cm ²)	Average FF $\pm \delta$ (%)	Average PCE $\pm \delta$ (%)	Series resistance R_S (Ω)	Shunt resistance R_p (Ω)
EA	1.00 \pm 0.02	23.23 \pm 0.20	69.31 \pm 3.77	16.16 \pm 0.94 17.12	68	2.74 E+5
EA, +KI	0.99 \pm 0.01	22.42 \pm 0.18	71.84 \pm 5.86	16.01 \pm 1.32 17.01	41	1.43 E+6
+DDABr	1.02 \pm 0.01	19.53 \pm 2.73	74.89 \pm 1.13	14.86 \pm 2.17 17.70	59	1.83 E+5
+DDABr, +KI	0.98 \pm 0.01	18.34 \pm 0.64	66.19 \pm 3.49	11.76 \pm 0.64 13.08	135	1.07 E+6
+NaLES	1.00 \pm 0.01	22.56 \pm 0.31	76.27 \pm 1.05	17.21 \pm 0.32 17.75	40	3.33 E+5
+NaLES, +KI	1.00 \pm 0.02	22.69 \pm 0.58	76.39 \pm 1.20	17.42 \pm 1.00 18.75	16	7.37 E+5
+NaLS	0.99 \pm 0.02	21.33 \pm 1.30	70.75 \pm 4.51	15.03 \pm 1.78 16.94	86	4.33 E+5
+NaLS, +KI	0.99 \pm 0.01	22.38 \pm 0.25	61.60 \pm 5.19	13.40 \pm 1.48 15.25	33	9.36 E+5
+(tBP)**	1.01 \pm 0.01	23.68 \pm 0.30	71.49 \pm 1.17	17.07 \pm 0.35 17.41	40	0.86 E+5

The perovskite thin films were prepared with different additives in EA anti-solvent solutions: DDABr, NaLES and NaLS, without or with KI as the additive in the perovskite precursor solutions. Series (R_S) and shunt (R_p) resistance of the PSCs were obtained from dark I - V curves of the corresponding PSCs

Bold values indicate the first and second best values in each column

*Concentration of the additive in EA anti-solvent solutions: 0.14 mg/mL, except in the case of EA+NaLS: 0.21 mg/mL

**4-Tertbutyl-pyridine (tBP), 8 μ mol in EA. Results from Table 2 of Ref. [25] for comparison purpose

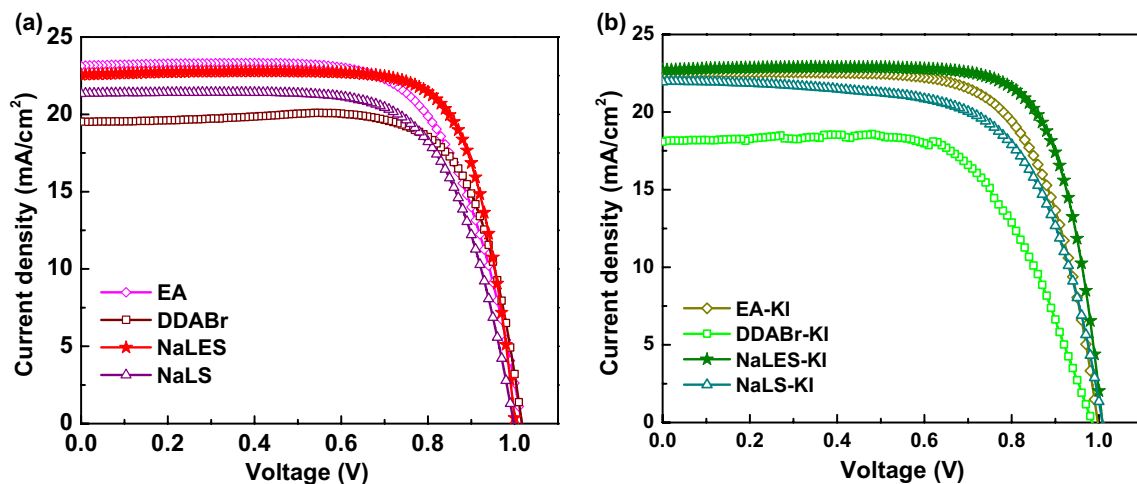


Fig. 7 Average current density (J) vs. voltage (V) curves of perovskite solar cells under illumination, prepared with four types of anti-solvent solutions: EA only, EA-DDABr, EA-NaLES and

EA-NaLS **a** without and **b** with the precursor solution additive KI (Color figure online)

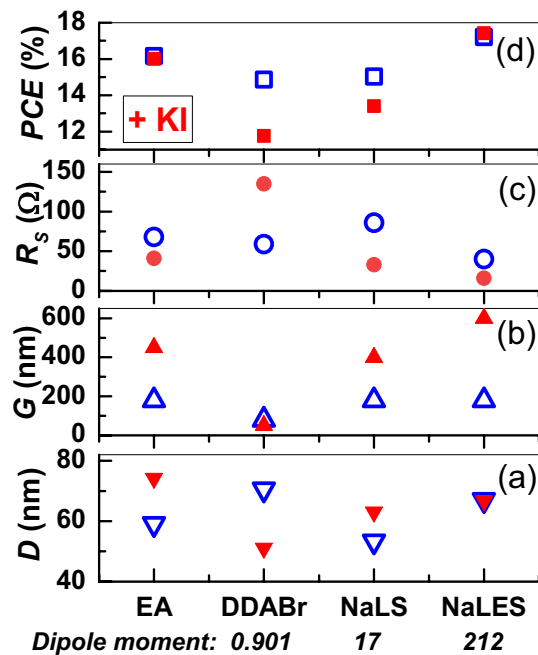


Fig. 8 Average **a** crystal (D) and **b** grain (G) size of perovskite thin films. **c** Series resistance (R_s) and **d** average power conversion efficiency (PCE) of the corresponding perovskite solar cells, prepared with different anti-solvent solutions: EA only, EA plus DDABr, NaLS or NaLES as additive. Red symbols: with KI in the perovskite precursor solutions (Color figure online)

in EA-KI and NaLES-KI-based PSCs. The reason for which the improved microscopic properties of perovskite films do not reflect in the average PCE of NaLS-based PSCs should be related to the less compact perovskite surface (Fig. 5d). The combination of KI with DDABr reduces the crystal and grain size of perovskite films, leading to the highest R_s and lowest PCE of the PSCs. Furthermore, the effect of NaLES and the combination of KI and NaLES can be observed in the increased external quantum efficiency (EQE) spectra of the corresponding PSCs in 490–790 nm wavelength region (Fig. S6a). This increase should come from an improved charge transport in the perovskite side of PSCs, which should be consequence of the increased crystal and grain size of perovskite thin films (Fig. 8).

It is worth mentioning the amount of KI in our perovskite precursor solutions is very small (5 μmol). Figure S6b shows the hysteresis index of each type of PSCs in Fig. 6. The addition of KI increases the hysteresis in EA-only, EA+ DDABr and EA+ NaLS perovskite solar cells. The exception is observed in the NaLES-based solar cells; the addition of KI slightly reduces the hysteresis index, from 14 to 11%. The results of

this work evidences that a small amount of KI in perovskite precursor solutions can cause morphology changes in air-processed perovskite thin films (Figs. 4, 5). These air-processed films should contain higher defect densities than perovskite samples prepared in an inert ambient, and probably such a small amount of KI is not sufficient to mitigate the hysteresis phenomena of the corresponding PSCs, as it did in those PSCs prepared under inert conditions [22, 23].

Finally, to see the stability of our air-processed unencapsulated PSCs, the eight types of PSCs shown in Fig. 6 were under continuous illumination for 30 min and their photovoltaic parameters were monitored to observe their stability under ambient conditions. Figure 9 shows the normalized (a) V_{OC} , (b) J_{SC} , (c) FF and (d) PCE values as functions of illumination time of PSCs prepared with EA-only and the three additives in EA anti-solvent solutions: DDABr, NaLES and NaLS. It is observed that without any anti-solvent additive, EA-only PSCs lose about 20% of their PCE after 30 min of continuous exposure to a solar simulator. Even with the addition of KI in the perovskite precursor solution, the stability of the EA-only PSCs was not improved (Fig. S7). Meanwhile, those PSCs with NaLES and NaLS anti-solvent additives lose about 12% of their PCE under the same conditions. The most stable PSCs were those prepared with the DDABr additive, maintaining around 95% of their original PCE after 30 min of continuous illumination, which should come from the very hydrophobic surface of DDABr-based perovskite films (Fig. 2b). The synergy of the KI perovskite precursor solution additive with EA anti-solvent additives to improve the stability of the corresponding solar cells is observed once again only in the case of NaLES; after 30 min of continuous illumination, PCE loss is reduced to 9% compared to its original PCE value (Fig. 9). For the rest of DDABr+KI and NaLS+KI cell samples, their stability does not improved with the addition of KI (Fig. S7).

To understand why NaLES provides the best photovoltaic performance of the air-processed PSCs, we look at the dipolar moment of the three anti-solvent additives. Although all of them are ionic surfactants and contain hydrophilic and hydrophobic terminal groups, they have very different dipole moment values (Table 1). The dipole moment of DDABr is about 0.907 D, similar to that of EA (0.331 D), however NaLS has the dipole moment of 17 D, and NaLES, 212 D, all estimated in dissociated state. A molecule with a larger dipole moment should exhibit a higher electric field to its neighborhood

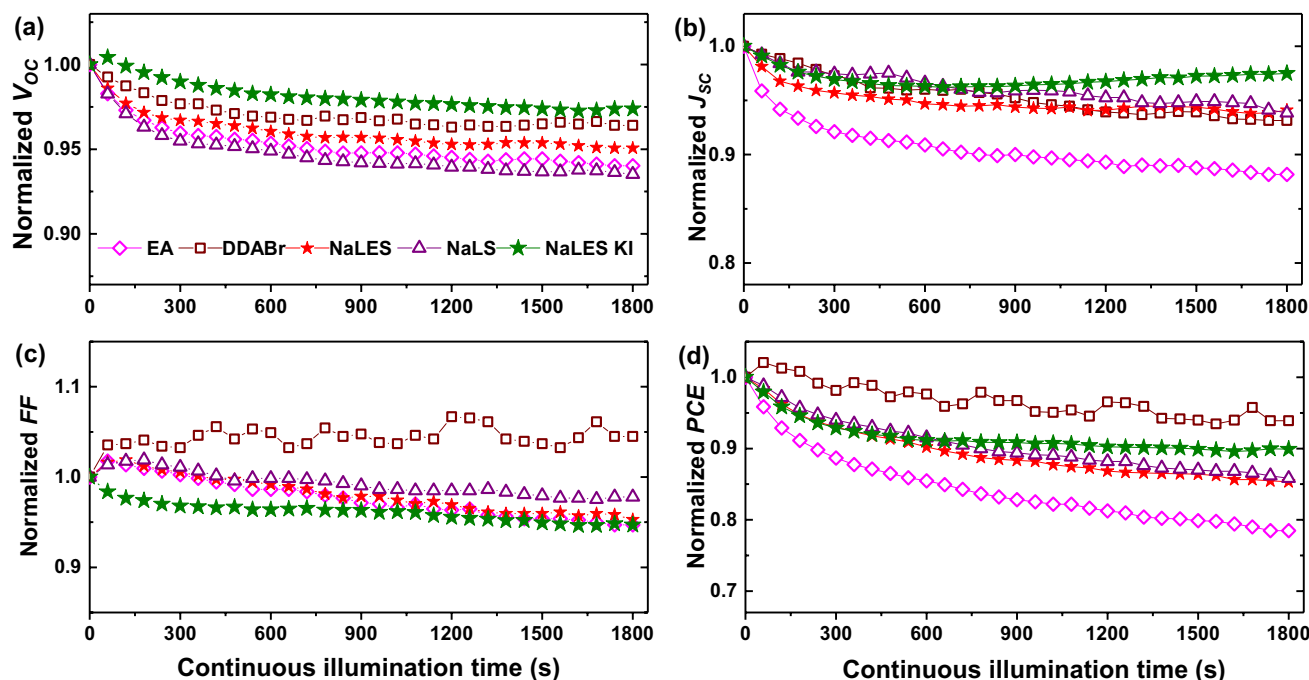


Fig. 9 Normalized **a** V_{oc} , **b** J_{sc} , **c** FF and **d** PCE values of perovskite solar cells as functions of illumination time, prepared with EA-only and additives in EA anti-solvent solutions: DDABr, NaLES and NaLS). The solid stars correspond to the perovskite

and be more effective to attract other polar molecules such as H_2O . It is reasonable to think that NaLES is more efficient to capture and remove the moisture from the perovskite precursor coating. With a lower content of water molecules, the perovskite compound would crystallize in larger sizes and form a more compact surface. On the other hand, DDABr with the lowest dipole moment creates a highly hydrophobic perovskite surface (Fig. 2b) to improve the stability of the PSCs. However, DDABr molecules in perovskite precursor coating impede the crystal growth and grain formation, resulting in larger series resistance and lower efficiency of the PSCs. Achieving an optimized combination of ionic surfactants of different dipole moments as anti-solvent additives for perovskite thin film preparation would be a good strategy to improve both the efficiency and stability of air-processed perovskite solar cells.

4 Conclusions

The results of this work confirm that the addition of di-dodecyl dimethylammonium bromide (DDABr), sodium lauryl ether sulfate (NaLES) or sodium lauryl

sulfate (NaLS) in ethyl acetate (EA) anti-solvent solutions impacts on the formation of air-processed $MAPbI_{3-x}Cl_x$ perovskite crystal size and surface morphology. The average power conversion efficiency (PCE) of NaLES-based perovskite solar cells (PSCs), compared to reference samples, increases from $16.16 \pm 0.94\%$ to $17.21 \pm 0.32\%$. Such improvement is related to the improved crystallinity and surface morphology of the perovskite thin films, consequence of a more efficient moisture extraction from precursor coatings by NaLES during the spin-coating process under ambient condition with a relative humidity of 44–53%. Furthermore, the synergy between NaLES and the perovskite precursor additive, KI, achieves the best photovoltaic performance of PSCs under ambient conditions, leading to an average PCE of 17.42% and the best PCE of 18.75%. Although the addition of DDABr and NaLS in EA anti-solvent solutions did not improve PCE of the PSCs, the efficacy of such additives is clearly observed in the stability improvement of the corresponding PSCs compared to the reference samples. The lowest dipole moment additive, DDABr, gives the highest hydrophobic perovskite surface, the lowest PCE and the lowest loss of PCE (5%) of the

corresponding PSCs after 30 min of continuous illumination under ambient conditions. An optimized combination of different surfactants as anti-solvent additives could improve both efficiency and stability of air-processed un-encapsulated PSCs.

Acknowledgements

The authors thank Maria Luisa Ramón-García for XRD measurement, Rogelio Morán-Elvira for SEM measurement and Gildardo Casarrubias-Segura for technical support in solar simulator and AFM measurement. JCC, MAMF, MCMV and CFAR acknowledge Consejo Nacional de Ciencia y Tecnología (CONACyT-México) for graduate scholarships. Financial support from UNAM-DGAPA-PAPIIT (IN104422) is acknowledged.

Author contributions

JC-C: conceptualization, methodology, investigation, data curation, writing—original draft. MAM-F: methodology, data curation, software, formal analysis. MCM-V: data curation, methodology. CFA-R: methodology. ANC-M: formal analysis. MAR-R: validation. MEN: writing—review & editing. MS-L: supervision. HH: conceptualization, investigation, writing—original draft, writing—review & editing, supervision, resources.

Funding

This study was funded by Dirección General de Asuntos del Personal Académico, Universidad Nacional Autónoma de México (Grant No. PAPIIT-IN104422).

Data availability

Data will be made available on request.

Declarations

Competing interests The authors declare that they have no known competing financial interests or personal relationships that could have appeared to influence the work reported in this paper.

Supplementary Information The online version contains supplementary material available at <https://doi.org/10.1007/s10854-023-11670-6>.

Open Access This article is licensed under a Creative Commons Attribution 4.0 International License, which permits use, sharing, adaptation, distribution and reproduction in any medium or format, as long as you give appropriate credit to the original author(s) and the source, provide a link to the Creative Commons licence, and indicate if changes were made. The images or other third party material in this article are included in the article's Creative Commons licence, unless indicated otherwise in a credit line to the material. If material is not included in the article's Creative Commons licence and your intended use is not permitted by statutory regulation or exceeds the permitted use, you will need to obtain permission directly from the copyright holder. To view a copy of this licence, visit <http://creativecommons.org/licenses/by/4.0/>.

References

1. A. Kojima, K. Teshima, Y. Shirai, T. Miyasaka, *J. Am. Chem. Soc.* **131**, 6050–6051 (2009). <https://doi.org/10.1021/ja809598r>
2. Best Research-Cell Efficiency Chart | Photovoltaic Research | NREL, <https://www.nrel.gov/pv/cell-efficiency.html>. Accessed 9 Mar 2023
3. G. Xing, N. Mathews, S. Sun, S.S. Lim, Y.M. Lam, M. Grätzel, S. Mhaisalkar, T.C. Sum, *Science* **342**, 344–347 (2013). <https://doi.org/10.1126/science.1243167>
4. J. Kim, A. Ho-Baillie, S. Huang, *Sol. RRL* **3**, 1800302 (2019). <https://doi.org/10.1002/solr.201800302>
5. I. Mesquita, L. Andrade, A. Mendes, *Sol. Energy* **199**, 474–483 (2020). <https://doi.org/10.1016/j.solener.2020.02.052>
6. Y. Cheng, X. Xu, Y. Xie, H.-W. Li, J. Qing, C. Ma, C.-S. Lee, F. So, S.-W. Tsang, *Sol. RRL* **1**, 1–8 (2017). <https://doi.org/10.1002/solr.201700097>
7. Y. Zhang, A. Kirs, F. Ambroz, C.-T. Lin, A.S.R. Bati, I.P. Parkin, J.G. Shapter, M. Batmunkh, T.J. Macdonald, Small

- Methods **5**, 2000744 (2021). <https://doi.org/10.1002/smt.202000744>
8. M. Younas, T.A. Kandiel, A. Rinaldi, Q. Peng, A.A. Al-Saadi, *Mater. Today Phys.* **21**, 100557 (2021). <https://doi.org/10.1016/j.mtphys.2021.100557>
9. B.G. Krishna, D. Sundar Ghosh, S. Tiwari, *Sol. Energy* **224**, 1369–1395 (2021). <https://doi.org/10.1016/j.solener.2021.07.002>
10. J. Song, Q. Hu, Q. Zhang, S. Xiong, Z. Zhao, J. Ali, Y. Zou, W. Feng, Z. Yang, Q. Bao, Y. Zhang, T.P. Russell, F. Liu, *Adv. Funct. Mater.* **31**, 2009103 (2021). <https://doi.org/10.1002/adfm.202009103>
11. M. Azam, K. Liu, Y. Sun, Z. Wang, G. Liang, S. Qu, P. Fan, Z. Wang, *J. Phys. D* **53**, 183002 (2020). <https://doi.org/10.1088/1361-6463/ab6f8d>
12. P. López-Mahía, S. Muniategui, D. Prada-Rodríguez, M.C. Prieto-Blanco, *Encyclopedia of Analytical Science*, 2nd edn. (Elsevier, Oxford, 2005), pp.554–561
13. W. Zhang, L. He, D. Tang, X. Li, *Sol. RRL* **4**, 2000376 (2020). <https://doi.org/10.1002/solr.202000376>
14. Y. Deng, X. Zheng, Y. Bai, Q. Wang, J. Zhao, J. Huang, *Nat. Energy* **3**, 560–566 (2018). <https://doi.org/10.1038/s41560-018-0153-9>
15. C. Li, J. Yin, R. Chen, X. Lv, X. Feng, Y. Wu, J. Cao, *J. Am. Chem. Soc.* **141**, 6345–6351 (2019). <https://doi.org/10.1021/jacs.9b01305>
16. Q. Wang, H. Li, J. Zhuang, H. Guo, X. Liu, Z. Guo, X. Gong, H. Li, *J. Mater. Sci.* **55**, 14761–14772 (2020). <https://doi.org/10.1007/s10853-020-05059-7>
17. I.-G. Bae, B. Park, *Sustain. Energy Fuels* **4**, 3115–3128 (2020). <https://doi.org/10.1039/d0se00598crsc.li/sustainable-energy>
18. K.-M. Lee, S.-H. Chan, C.-C. Ting, S.-H. Chen, W.-H. Chiu, V. Suryanarayanan, J.-F. Hsu, C.-Y. Liu, M.-C. Wu, *Nanomaterials* **12**, 2651 (2022). <https://doi.org/10.3390/nano12152651>
19. K. Liu, Q. Liang, C. Lee, G. Li, *Joule* **4**, 2404–2425 (2020). <https://doi.org/10.1016/j.joule.2020.09.011>
20. J. Zhu, Y. Qian, Z. Li, O.Y. Gong, Z. An, Q. Liu, J.H. Choi, H. Guo, P.J. Yoo, D.H. Kim, T.K. Ahn, G.S. Han, H.S. Jung, *Adv. Energy Mater.* **12**, 2200632 (2022). <https://doi.org/10.1002/aenm.202200632>
21. Z. Tang, T. Bessho, F. Awai, T. Kinoshita, M.M. Maitani, R. Jono, T.N. Murakami, H. Wang, T. Kubo, S. Uchida, H. Segawa, *Sci. Rep.* **7**, 12183 (2017). <https://doi.org/10.1038/s41598-017-12436-x>
22. D.Y. Son, S.G. Kim, J.Y. Seo, S.H. Lee, H. Shin, D. Lee, N.-G. Park, *J. Am. Chem. Soc.* **140**, 1358–1364 (2018). <https://doi.org/10.1021/jacs.7b10430>
23. D.-H. Kang, N.-G. Park, *Adv. Mater.* **31**, 1805214 (2019). <https://doi.org/10.1002/adma.201805214>
24. J. Li, X. Hua, F. Gao, X. Ren, C. Zhang, Y. Han, Y. Li, B. Shi, S. Liu, *J. Energy Chem.* **66**, 1–8 (2022). <https://doi.org/10.1016/j.jechem.2021.06.023>
25. C.F. Arias-Ramos, Y. Kumar, P.G. Abrego-Martínez, H. Hu, *Sol. Energy Mater. Sol. Cells* **215**, 110625 (2020). <https://doi.org/10.1016/j.solmat.2020.110625>
26. S. Rahimnejad, A. Kovalenko, S.M. Forés, C. Aranda, A. Guerrero, *ChemPhysChem* **17**, 2795–2798 (2016). <https://doi.org/10.1002/cphc.201600575>
27. T. Raboekai, *Físico-química de superficies* (The General Secretariat of the Organization of American States, Washington DC, 2014), p.14
28. W.H. Hall, *Proc. Phys. Soc. Lond. Sect. A* **62**, 741–743 (1949). <https://doi.org/10.1088/0370-1298/62/11/110>
29. G.K. Williamson, R.E. Smallman, *Philos. Mag.* **1**, 34–46 (1956). <https://doi.org/10.1080/14786435608238074>
30. M. Khitouni, M. Mhadhbi, L. Escoda, J.J. Suñol, M. Dammak, *J. Nanomater.* **2010**, 712407 (2010). <https://doi.org/10.1155/2010/712407>
31. K. Venkateswarlu, M. Sandhyarani, T.A. Nellaippan, N. Rameshbabu, *Procedia Mater. Sci.* **5**, 212–221 (2014). <https://doi.org/10.1016/j.mspro.2014.07.260>
32. B.E. Warren, *X-Ray Diffraction* (Dover Books on Physics, New York, 1968)
33. R. Rai, T. Triloki, B.K. Singh, *Appl. Phys. A* **122**, 774 (2016). <https://doi.org/10.1007/s00339-016-0293-3>
34. H. Kafashan, *J. Electron. Mater.* **48**, 1294–1309 (2019). <https://doi.org/10.1007/s11664-018-6791-7>

Publisher's Note Springer Nature remains neutral with regard to jurisdictional claims in published maps and institutional affiliations.